공학석사 학위논문

Development of quinone based new electrode additives for improved pseudocapacitance

축전용량 향상을 위한 퀴논 기반 새로운 전극 첨가제 개발

2022 년 2 월

서울대학교 대학원

융합과학부 나노융합전공

이 규 철

Development of quinone based new electrode additives for improved pseudocapacitance

지도 교수 이 강 원

이 논문을 공학석사 학위논문으로 제출함
2022 년 01 월

서울대학교 대학원
융합과학부 나노융합전공
이 규 철

이규철의 공학석사 학위논문을 인준함
2022 년 01 월

위 원 장 박 원 철 (인)

부위원장 이 강 원 (인)

위 원 고 장 면 (인)

Abstract

Development of quinone based new electrode additives for improved pseudocapacitance

Kyuchul Lee
Program in Nano Science and Technology
Graduate School of Convergence Science & Technology
Seoul National University

Redox active organic compounds have proven to be functional materials for devices such as switches, molecular wires, sensors and, importantly, electronic/optoelectronic devices. These organic molecules are functionalized with various redox active substances that can undergo redox reactions. Among these compounds, quinone-based materials have received considerable attention as an electrode material for an energy storage device because they are cost-effective, environmentally friendly and exhibit high

reversibility.

In this study, quinone-based derivatives are synthesized and then blended physically with activated carbon. Three quinone based derivatives (HBU 680, HBU 888, and HBU 889) are synthesized and used as electrode additives for supercapacitors. Organic additives including activated carbon and their complexes are primarily characterized by a PhQ-$PhQH_2$ redox transition involving a two-electron two-proton process. The composite electrodes show specific capacitance of 176 F/g, 262 F/g, and 145 F/g for HBU 680, HBU 888 and HBU 889 respectively at current density 5 mA/cm^2. Cycle performance can also be enhanced by the adoption of $PhQH_2^-$ based organic additives for their pore-filling morphology to increase the packing density of composite electrodes. The composite electrodes also show 100% capacity retention over 10,000 cycles. These results show that the new quinone-based derivates can enhance pseudocapacitive behavior and warrant their use as electrode addiitves for supercapacitors.

The quinone derivatives were obtained by a simple one or two-pot synthesis process using less harmful organic solvents. A coating slurry using activated carbon as an active material, quinone derivatives as a redox additive, polyvinylidene fluoride as a polymer

binder, and N-methyl-2-pyrrolidinone as a dispersion solvent was perfectly mixed to provide an excellent composite electrode as shown by the SEM data. The cyclic voltammetry performed in a three-electrode cell using a composite electrode as the working electrode of 1 M H_2SO_4 showed a high potential window in the -0.2 ~ 0.8 V range and good capacitance retention compared to Ag/AgCl. The experimental results showed that the capacitive performance of the composite electrode is due to the synergistic effect between activated carbon and organic additives. This effective method can be used to obtain good performing composite electrodes for supercapacitor applications.

Keywords: Quinone-based, Activated Carbon, Redox reaction, Pseudocapacitance.

Student Number: 2017-22884

Table of Contents

List of Figures

List of Tables

Chapter 1. Introduction

1.1. Historical overview of supercapacitors

In recent decades a serious demand for energy usage for basic and more complex but vital applications, puts a lot of pressure on the scant traditional non-renewable resources like oil and coal to the detriment of our life and our environment. To address these issues, a general shift is seen from total dependence on traditional non-renewable energy sources to a sustainable renewable energy. In most cases the general procedure employed is to store excess energy generated during peak power for reuse. This conservative science has received tremendous interest that allows for research to explore into energy storage devices for daily applications. Supercapacitors and batteries contribute to the major energy storage devices operating through electrochemical mechanism. Batteries can be further classified into two broad categories which are primary batteries and secondary/rechargeable batteries [1]. Supercapacitors can be put into three main folders namely; Electric double-layer capacitors (EDLCs), Redox capacitors and Hybrid capacitors [2]. Despite differences in the energy storage and conversion mechanisms, a few similarities remain amongst these

two storage devices. In both devices, electron and ion transport are separated with the energy-generating process occurring at the electrode/electrolyte interphase [3]. Originally the battery generates its energy by a faradaic redox mechanism whiles energy storage by supercapacitors are made possible by the formation of electric double layers, fast faradaic reactions or a combination of both [2]. As a result of this mechanisms, supercapacitor is able to release its energy faster than the battery hence its relative higher power output. Lacking though is the small amount of energy that can be stored by EDL process. It is also evident that the supercapacitor has a longer cycle life because of the ease with which the EDL formation occurs [2]. The application of these two devices alters widely different fields. For power devices that require quick energy consumption over a short period like power drills, photographic flashes for digital cameras and defibrillators, the supercapacitor is best suited for their use [2]. On the other hand, batteries find uses as the main energy supplier in portable electronics like smart phones, laptop pcs and electric vehicles to mention but a few. It is clear that despite the qualities possessed by these two devices, single handedly, none has the characteristics to surpass the high energy and power output of internal combustion engines [3].

1.2. Design and fundamental concepts of supercapacitors

Electrolytic capacitors are the latest progress in the technology of the capacitor, in which the dielectric is replaced with an ionic electrolyte [4−6]. Within the electrolytic capacitor, the ions can be transferred freely in the electrolyte, creating at the electrode/electrolyte interface a much larger charge density than that created at the interface of electrode/dielectric [6]. Consequently, the capacitance of electrolytic capacitors is often measured by mF, whereas those of dielectric capacitors in the μF range [4]. Supercapacitors in which instead of using conventional dielectrics between the plates, use an electrolyte that ionically bridges between the two electrodes which are separated by an ion−permeable substance [7]. In supercapacitors, the charge storage process is classified into Electric−double−layer capacitors (EDLCs) that describe the materials in which the charge is separated forming “Helmholtz double−layer” and electrostatically adsorbed at the electrode/electrolyte interface creating a potential differences between the two electrodes which means that no electron shift between the electrolyte and the electrodes [8−14].

The first EDLC was manufactured in 1957 by General Electric

using its plates made of activated charcoal [15]. The second type was known as pseudocapacitors, which involved a capacitive–fradaic process that describes the material in which the electrochemical behavior is capacitive in nature but storing the charge happens by charge–shifting faradaic reactions within the double layer especially when using redox electrolyte supplying a high Cs compared to EDLCs [16,17]. The first explored pseudocapacitors material was RuO_2 by B. E. Conway. The materials that exhibit redox behavior and utilized in pseudocapacitors such as CoS, MnS, NiS, etc., and conducting polymers such as polyaniline, polythiophene, polypyrrole (PPy), polyvinyl alcohol (PVA), etc [15]. The last type of materials used in supercapacitors was known as battery–type that involves a non–capacitive faradic performance and nature [15]. The nature of electrode material such as its affinity to adsorb ions on its surface in addition to its texture nature controls the electrochemical behavior of this material. Consequently, since 2000, the dramatic growth of nanoscience and progressive characterization methods has witnessed a significant increase in the amount of research related to supercapacitors following the emergent increased request for high–energy, high–power, and benign energy–storage systems [18].

1.3. Energy storage mechanism in supercapacitors

1.3.1. Electric-double-layer capacitance (EDLCs)

EDLCs store charges directly across the double layer of the electrode and there is no charge transfer across the interface that is true capacitance effect. Because this layer is formed by the physical movement of ions, there is no chemical reaction involved as there is with batteries. This gives the supercapacitor a superior charge-discharge cycle life. While excess or deficiency of charge builds up on the electrode surface, ions of the opposite charge build up in the electrolyte near the electrode/electrolyte interface in order to provide electro-neutrality. Helmholtz first modeled and described the EDL concept in the 19th century during the investigation of a colloidal particles interface [19]. The model which is similar to a conventional capacitor states two parallel layers established at the electrode-electrolyte interface with an atomic distance separation.

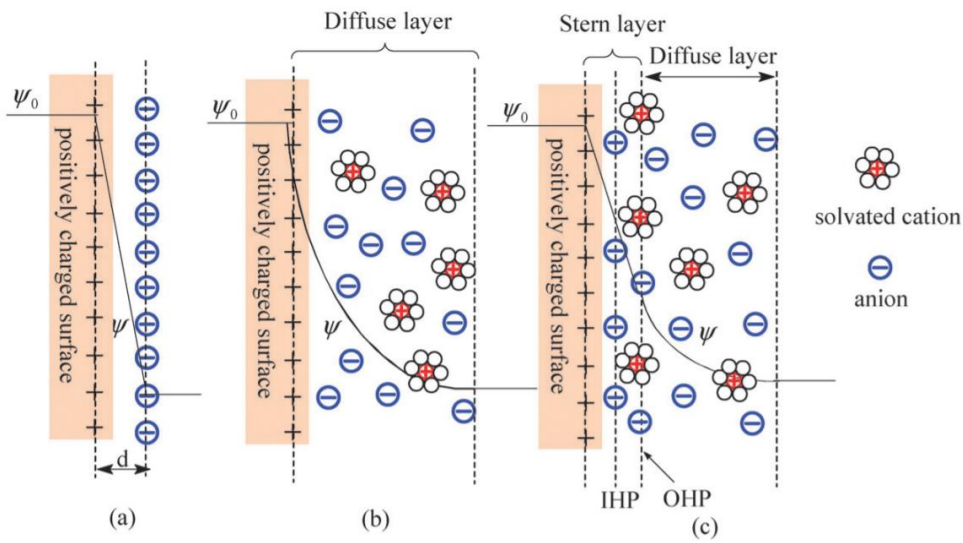

Figure 1. Model of the electric double layer: (a) Helmholtz model (b) Gouy point charge model (c) Stern model for finite ion size with thermal distribution [20].

The capacitance in the EDL (C_{dl}) can be treated as a combination of the capacitances from two regions, the Stern type of compact double layer capacitance (C_H) and the diffusion region capacitance (C_{diff}). Thus, C_{dl} can be expressed by the following equation:

$$\frac{1}{C_{dl}} = \frac{1}{C_H} + \frac{1}{C_{diff}}$$

The factors that determine the EDL behavior at a planar electrode surface include the electrical field across the electrode, the types of electrolyte ions, the solvent and the chemical affinity between the adsorbed ions and the electrode surface. As the electrode is usually a porous material with a high specific surface area, the EDL behavior at the pore surface of the porous electrode is more complex than that at an infinite planar one as the ion transportation in a confined system can be drastically affected by a number of parameters, such as the tortuous mass transfer path, the ohmic resistance associated with the electrolyte, and the wetting behavior of the pore surface by the electrolyte.

1.3.2. Pseudocapacitors

Unlike EDL capacitance, pseudocapacitance arises for thermodynamics reasons and is due to charge acceptance (Δq) and a change in potential (ΔV) [21]. The derivative C = d(Δq)/(dΔV) corresponds to a capacitance, which is referred to as the pseudo-capacitance. The main difference between pseudocapacitance and EDL capacitance lies in the fact that pseudocapacitance is faradic in origin, involving fast and reversible redox reactions between the electrolyte and electro-active species on the electrode surface. The most commonly known active species are ruthenium oxide, manganese oxide, vanadium nitride, electrically conducting polymers such as polyaniline, and oxygen or nitrogen containing surface functional groups [22-26]. While pseudocapacitance can be higher than EDL capacitance, it suffers from the drawbacks of a low power density due to poor electrical conductivity, and lack of stability during cycling. The pseudocapacitive behavior of ruthenium oxide, RuO_2, is widely investigated. The electrochemical reaction of RuO_2 electrodes can be described as a fast, reversible, and redox behavior as the following reaction $RuO_2 + nH^+ + ne^- \leftrightarrow RuO_2-n(OH)_n$ [27].

However, high ruthenium costs limited their applications to a number of high-value electronic equipment. Academic institutions have focused on searching for other materials cheaper than RuO_2, such as other transition metal oxides (iron, vanadium, nickel, and cobalt) and/or their corresponding sulfides. A suitable alternative to RuO_2 appears to be manganese oxides with relatively low costs, low toxicity, environmental benignity, and potentially high theoretical capacitance up to 1300 F/g.

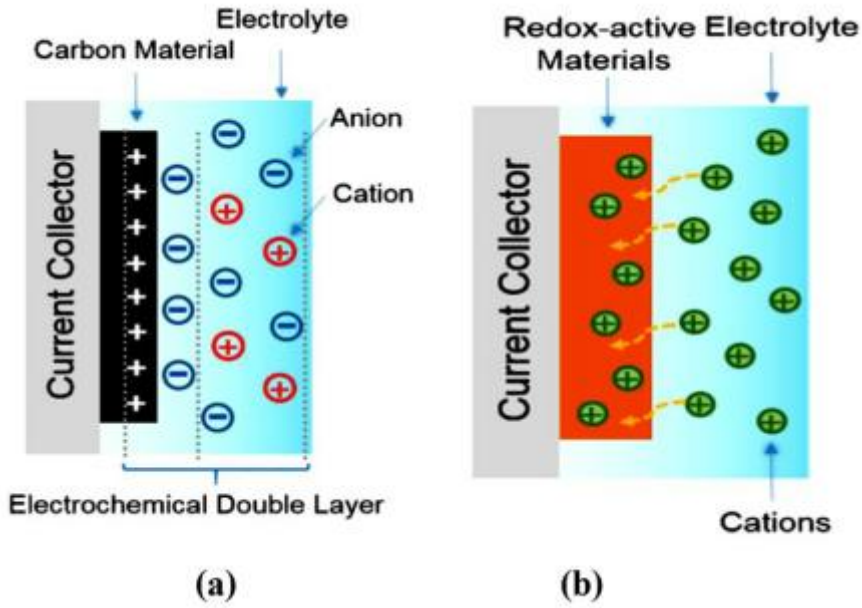

Figure 2. Different electrochemical energy storage materials (a) EDLC, (b) Pseudocapacitor [28].

1.4. Requirements for electrode material

Materials judged to be suitable as electrode materials for supercapacitors should satisfy the following criteria:

1. Long stable cycle life ($>10^5$ charge/discharge cycle).
2. The surface area should be high ($>10^3$ m^2/g).
3. Pore size evenly distributed in material.

Long cycle life allows supercapacitors to be continuously charged and discharged to meet the energy and power demands of devices using supercapacitors. The high active surface area makes it possible to achieve high specific capacitance supercapacitors and devices with lower weight. The well-controlled pore size and pore distribution allow the electrolyte materials to reach the active surface area and cavities of the electrode material.

1.5. Materials for supercapacitors' electrodes

1.5.1. Carbon-based materials

Activated carbons (ACs) are the mostly widely used electrode materials due to their large surface area, relatively good electrical properties and moderate cost. ACs are generally produced from physical, thermal and chemical activation of various types of carbonaceous materials (e. g. coal, nutshell, wood, etc.). Physical activation usually refers to the processing of carbon precursors at high temperatures in the presence of oxidizing gases such as steam, CO_2 and air. Chemical activation is usually performed at lower temperatures using activators such as phosphoric acid, potassium hydroxide, sodium hydroxide and zinc chloride. Depending on the activation method and the carbon precursor used, ACs with various physicochemical properties with a well-developed surface area of 3000 m^2/g were produced and their electrochemical properties were studied [29-35]. In addition to the porous structure of AC, the surface function plays an important role in carbon electrode performance as it affects the wettability of the carbon surface by electrolyte ions and provides an additional pseudocapacitance

[35,36]. An activated carbon containing a high concentration of oxygen-functional groups with low porosity (BET specific surface area = 270 m^2/g) has been prepared by one-step carbonization of an oxygen-rich carbon precursor [35]. However, most commercial supercapacitors use organic electrolytes because of the higher operating voltages, which offer a higher energy density. Pandolfo and Hollenkamp have given an overview of ACs with various types of functional groups and pointed out that the presence of some active surface oxides and a trace amount of water result in instability of the electrode, an increase of series resistance and the decomposition of the organic electrolyte [36].

Carbon nanotubes can be categorized as single-walled carbon nanotubes or multi-walled carbon nanotubes, both of which have been widely explored as energy storage electrode materials. Carbon nanotubes are generally considered the choice of high-power electrode materials because of their excellent electrical conductivity and easily accessible surface area. It also provides good support for active materials due to its high mechanical elasticity and open tubular network. However, energy density is problematic due to its relatively small specific surface area (typically ~500 m^2/g) compared to ACs. More importantly, the difficulty of maintaining the intrinsic properties of individual Carbon

nanotubes on the macroscopic scale and their high purity and electrolyte dependent capacitance performance [38,39].

Graphene is a one-atom thick sheet of graphite in which the atoms are arranged in a hexagonal pattern. They have a theoretical specific surface area of 2630 m^2/g, resulting in theoretical capacitance of 550 F/g. They are highly conductive compared to activated carbon [40].

1.5.2. Pseudocapacitive electrode materials

Faradaic pseudocapacitance occurs with static double-layer capacitance. The quantity of pseudocapacitance is dependent on the surface area, material and the electrode structure. The amount of charge stored in pseudocapacitance is directly proportional to the applied voltage. The electrode material chemical similarity to the ions adsorbed on the electrode surface and pore structure determines the ability of the electrode to exhibit quasi-capacitive behavior. Materials considered to exhibit redox behavior include transition metals, conductive polymers, and some organic molecules. The fast and modifiable oxidation and reduction reactions exhibited by conductive polymers can be attributed to the available π-conjugated polymer chains. During oxidation, ions are transferred to the polymer backbone and released back to the electrolyte during reduction [41]. Conducting polymer include Polyacetylene, polyaniline [42], polypyrrole [43], and polythiophene. Conducting polymers uses electrochemical doping or de-doping of the polymer including anions and cations. High capacitance and power density are obtained with one negatively charged (n-doped) and the other which is positively charged (p-doped) electrode. Conducting

polymer materials exhibit poor cycle life due to volume change or swelling as a result of doping ions. Their conductive nature is due to the delocalization of elections in the conjugated chemical bond along the polymer backbone [44].

Chapter 2. Experimental Section

2.1. Synthesis of quinone based derivatives

Quinone-based materials have attracted considerable attention as electrode materials for energy storage because they are cost effective, environmentally friendly and exhibit high reversibility [45]. They have been discovered to provide theoretical capacitance comparable to lithium ion batteries [46]. Various methods have been developed on how to combine quinone species and carbon materials to enhance the charge storage performance of carbon. These include grafting reaction via diazonium chemistry [47,48], polymerization [49], and adsorption [50].

2.1.1 Synthesis of HBU 889

Hydroquinone (200 mg, 1.82 mmol) was dissolved in EtOH, and $CeCl_3$ $7H_2O$(67mg, 0.18mmol) was added. Subsequently, after adding 2,3,4-trimethoxy benzylpiperazine (1.24 g, 3.64 mmol) under an ice bath, TEA (1.27ml, 9.1mmol) was added dropwise. After overnight and concentration under reduced pressure, the reaction was terminated using H_2O under an ice bath. Afterwards, the brown solid was obtained through filtering (750 mg, 64.72 % yield). The synthesized HBU 889 was analysed using ^{1}H and ^{13}C nuclear magnetic resonance spectroscopy (Varian Gemini 200 NMR). ^{1}H NMR(400 MHz, DMSO) 3.03 (t, J = 7.6 Hz, 2H), 3.48 (q, J = 6.8 Hz ^{1}H NMR (400 MHz, $CDCl_3$) δ 2.56 (s, 8H), 3.49 (s, 4H), 3.55 (s, 8H), 3.85 (s, 6H), 3.87 (d, J=3.6, 12H), 5.50 (s, 2H), 6.63 (d, J= 8.4, 2H), 6.96 (d, J= 8.4, 2H); ^{13}C NMR ($CDCl_3$, 100MHz) δ 48.92(2C), 52.54 (2C), 56.00 (2C), 56.41 (1C), 60.81 (2C), 61.22 (2C), 76.74 (4C), 77.06 (4C), 77.37 (4C), 106.55 (1C), 106.99 (2C), 123.41 (1C), 125.16 (2C), 142.34 (1C), 152.34 (2C), 153.09 (1C), 182.68 (1C); ESI-MS: m/z [M]+ 637.3 (calcd. 636.74).

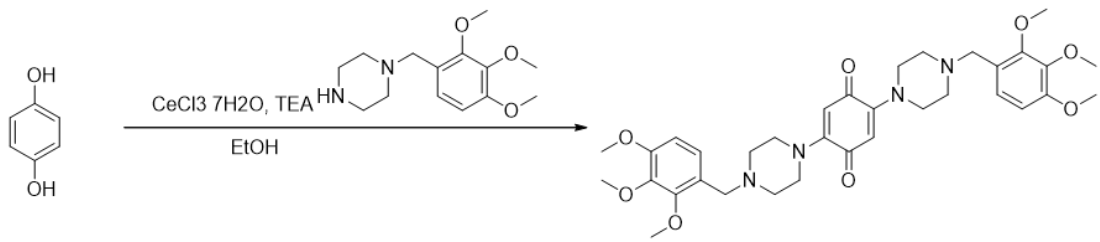

HBU 889

Figure 3. Structure and synthesis reaction of the HBU 889.

2.1.2 Synthesis of HBU 888

1,4,−dihydroxy naphtalene (200 mg, 1.20 mmol) was dissolved in ethanol, and $CeCl_3$ $7H_2O$ (45 mg, 0.12 mmol) was added. Subsequently, after adding 2,3,4−trimethoxybenzyl piperazine (410 mg, 1.20 mmol) under an ice bath, TEA (500 μl, 3.6 mmol) was added dropwise. After overnight and concentration under reduced pressure, the reaction was terminated using H_2O under an ice bath. After filtering the solid, the obtained solid was dissolved in acetone, concentrated under reduced pressure, and recrystallized from ether. The crude liquid was collected and concentrated under reduced pressure by column chromatography (DCM→DCM:MeOH=19:1) to obtain (dark red liquid, 76 mg, 14.99 % yield). The synthesized HBU 888 was analysed using ^1H and ^{13}C nuclear magnetic resonance spectroscopy (Varian Gemini 200 NMR). TLC [EA:HEX=1:1 Rf = 0.4; ^1H NMR (400 MHz, $CDCl_3$) δ 2.63(t, J= 4.8Hz, 4H), 3.51~3.53 (m, 6H), 3.86 (s, 3H), 3.88 (s, 3H), 3.90 (s, 3H), 6.00 (s, 1H), 6.65(d, J=8.8Hz, 1H), 6.99(d, J=8.4Hz, 1H), 7.62 (td, J= 1.2Hz, J =7.6Hz, 1H), 7.63 (td, J= 1.2Hz, J=7.6Hz, 1H), 7.99 (dd, J =0.8Hz, J =7.6Hz, 1H), 8.03 (dd, J= 0.8Hz, J =7.6Hz, 1H); ^{13}C NMR ($CDCl_3$, 100MHz) δ 49.03 (2C), 52.42

(2C), 55.99 (1C), 56.43 (1C), 60.80 (1C), 61.22 (1C), 107.00 (1C), 111.47 (1C), 123.30 (1C), 125.17 (1C), 125.52 (1C), 126.65 (1C), 132.40 (1C), 132.84 (2C), 133.83 (1C), 142.34 (1C), 152.67 (1C), 153.12 (1C), 153.80 (1C), 183.11 (1C), 183.64 (1C); ESI-MS: m/z [M]+ 423.2 (calcd. 422.18).

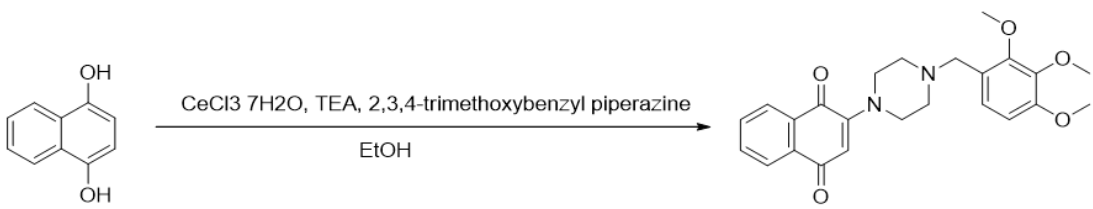

HBU 888

Figure 4. Structure and synthesis reaction of the HBU 888.

2.1.3 Synthesis of HBU 680

3-Methoxybenzyl bromide (0.19 mL, 1.27 mmol) was dissolved in 10mL of DMSO, and NaN_3 was added in small portions. Subsequently, the mixture was stirred at room temperature for 24 h. After terminating the reaction with H_2O, the organic layer was extracted with ether. The extracted organic layer was filtered under reduced pressure after water removal with anhydrous $MgSO_4$ to obtain a solution. This was concentrated under reduced pressure to obtain a colorless liquid. (150mg, 92%). The synthesized 1-(azidomethyl)-3-methoxybenzene was analysed using ^1H nuclear magnetic resonance spectroscopy (Varian Gemini 200 NMR). ^1H NMR ($CDCl_3$, 400MHz) : δ 3.80 (s, 3H), 4.29 (s, 2H), 6.85 ~ 6.89 (m, 3H), 7.28 (t, J = 8.0 Hz, 1H).

6-(ethynylamino)-6H-dibenzo[c,e][1,2]oxaphosphinine 6-oxide (0.20g, 0.74mmol) was dissolved in acetone solvent, then $Cu(PPh_3)_3Br$ (0.07 g, 0.074 mmol) and 1-(Azidomethyl)-3-methoxybenzene (0.13 g, 0.82 mmol) were added into the solution. Subsequently, the mixture was reacted in a microwave at 90℃ for 4h. After separation by column chromatography (DCM: MeOH 40:1), a brown solid (260 mg, 81% yield) was obtained. The synthesized

HBU 680 was analysed using ^{1}H and ^{13}C nuclear magnetic resonance spectroscopy (Varian Gemini 200 NMR). ^{1}H NMR (DMSO-d_6, 400MHz) δ 3.75 (s, 3H), 4.09 (d, J = 7.2 Hz, 1H), 4.13 (d, J = 7.2 Hz, 1H) 5.55 (s, 2H), 6.24 (m, 1H), 6.89 (d, J = 7.6 Hz, 1H), 6.93 (t, J = 2.4 Hz, 2H), 7.16 (d, J = 8.0 Hz, 1H), 7.20 (d, J = 6.8 Hz, 1H), 7.33 (d, J = 7.6 Hz, 1H) 7.42 (t, J = 8.0 Hz, 1H), 7.51 (td J = 2.8, 7.6 Hz, 1H), 7.74 (d, J = 7.6 Hz, 1H), 7.77 (d, J = 7.6 Hz, 1H) 7.98 (s, 1H), 8.16 ~ 8.21 (m, 2H); ^{13}C NMR (DMSO-d_6, 100MHz) δ 36.30, 53.16, 55.61, 113.86, 114.37, 120.56 (d, J = 6.0 Hz), 120.58, 122.46 (d, J = 12.0 Hz), 123.57, 124.53 (d, J = 10.0 Hz), 124.75, 125.90, 125.92 (d, J = 161.0 Hz), 128.75, 130.04 (d, J = 10.0 Hz), 130.38, 130.82, 133.21, 133.23, 136.45 (d, J = 7.0 Hz), 138.04, 149.89 (d, J = 7.0 Hz), 159.94 Melting point (℃) 50℃; ESI-MS : m/z $[M+H]^{+}$ 433.2(calcd. 432.14).

(a)

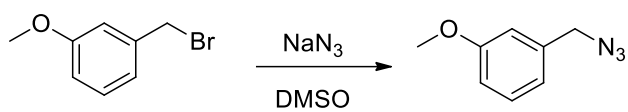

(b)

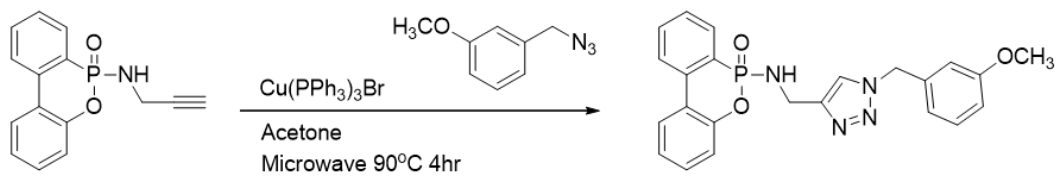

HBU-680

Figure 5. (a) Synthesis reaction of the 1-(azidomethyl)-3-methoxybenzene (b) Structure and synthesis reaction of the 6-(((1-(3-methoxybenzyl)-1H-1,2,3-triazol-4-yl)methyl) amino)-6H-dibenzo[c,e] [1,2]oxaphosphinine 6-oxide (HBU 680).

2.2. Redox mechanisms of the HBU additives

The HBU 680 has a redox reaction at the O atom double-bonded to the P on the DOPO PP as and on the middle N atom in the triazole structure. The more electronegative N pulls electrons from the double bond towards itself resulting in a partial negative charge where the H^+ ion can reversibly bond to make a secondary amine group (NH group) [51,52]. The oxide ion bonded to P due to resonance will become a hydroxyl anion. This enhances the specific capacitance compared to pure AC. However, it has the lowest specific capacitance compared to the other HBU additives due to the slowness of the redox reactions on the redox-active sites (the P=O and =N－N=N－). The basicity of phosphoxide and the aromatic N is lower compared to that of the phenoxide anion formed by the quinone moiety. The HBU 889 has quinone-hydroquinone ($Q-QH_2$) transitions with hydroquinone in an acidic medium. There are no aromatic N atoms but two 2,3,4-trimethoxybenzylpiperazine groups directly bonded to the quinone moiety. The piperazine nitrogen atoms are electron-withdrawing since they are tertiary N atoms [53, 54]. This destabilizes the quinone π-system thereby

reducing its basicity resulting in reduced rate of the $Q-QH_2$ transition. However, HBU 888 displayed the highest specific capacitance. Like HBU 889 which has $PhQ-PhQH_2$ transitions, however, the side groups on the quinone moiety are different. It has one 2,3,4-trimethoxybenzylpiperazine group thus less electron-withdrawing hence more basic than HBU 889 [51]. The redox mechanisms of the HBU samples are shown in Figure 6.

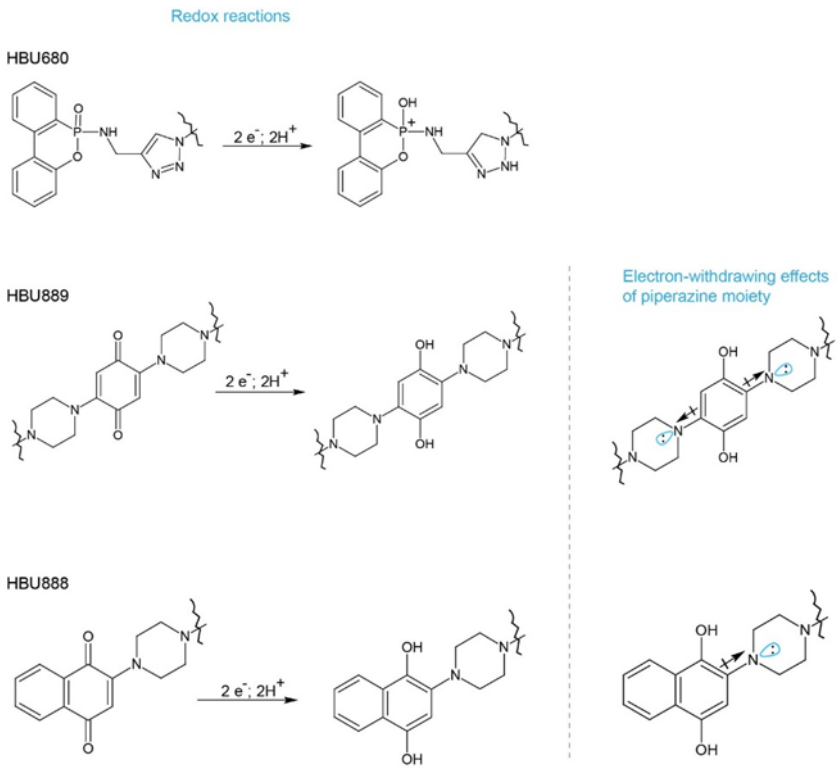

Figure 6. Redox mechanisms of the HBU additives.

2.3. Composite electrode preparation

HBU 680, HBU 888 and HBU 889 were used as a redox additives separately for supercapacitor electrodes. The viscous electrode slurry was prepared by mixing AC (MSC-30, Kansai Cokes, 70 wt.%), synthesized quinine-based additives (25 wt.%) and polymeric binder (polyvinylidene fluoride (Aldrich, 5 wt.%) and N-methyl-2-pyrrolidinone as the dispersion solvent. The viscous slurry for each sample was coated on platinum current collectors (1.0 cm × 1.0 cm) and dried at 100℃ in an oven for 4h.

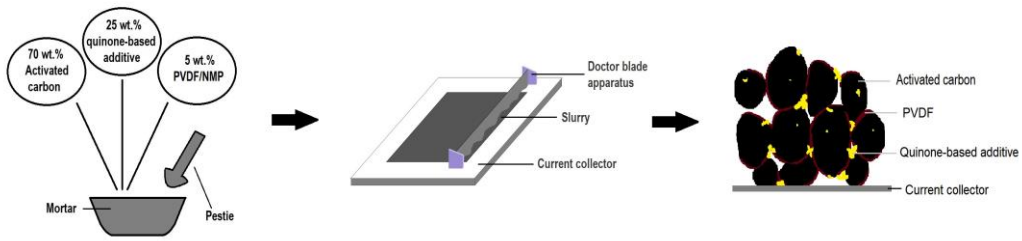

Figure 7. Systematic procedure for the electrode preparation.

2.4. Electrochemical characterization

For the cyclic voltammetry measurement of the electrodes, a three-electrode cell was used. This is equipped with a reference electrode made up of Ag/AgCl saturated with KCl, platinum as a counter electrode, and the composite as a working electrode. The aqueous electrolyte solution used 1M H_2SO_4 (Autolab (PGstat 100, Eco Chemie). Different scan rates of 100~1000 mV/s were used and the potential range was from −0.2 to 1.0 V vs. Ag/AgCl. The specific capacitance (Cs) of the redox additives was calculated as a function of scan rate. The equation used for calculation was

$$Cs = \frac{[Q1 + Q2]}{2m\Delta V}$$

Where Cs is the specific capacitance, Q1 anodic charge, Q2 cathodic charge, ΔV is the potential window used and m mass of active material.

Galvanostatic charge-discharge was carried out at different current densities of 5, 7 and 10 mA/cm^2 for HBU 680 and HBU 888. For HBU 889 the current densities used were 5 and 7 mA/cm^2. The voltage range of −0.2~0.8V (vs Ag/AgCl) using a cycler (Toscat3000, Toyo systems) was used for the CD analysis.

Chapter 3. Results and Discussion

3-1. Characterization of quinone based composite electrode

Brunauer-Emmett-Teller (BET) analysis and Scanning electron microscopy (SEM) images were done using a Hitachi S-4800 field emission scanning electron microscopy (FESEM) and a Tristar II 3020 Micromeritics instrument respectively. Table 1 presents the summary of the surface area, pore-volume, and pore size of the different samples. The surface area follows the trend HBU888 > HBU680 > HBU889 > AC. The enhanced specific surface area leads to (i) improved ion migration, (ii) more active sites for EDLC and redox processes hence enhanced electrochemical performance [55, 56]. The N_2 adsorption-desorption isotherm was used to determine the pore size and specific surface area of the as-prepared AC (Figure 8). The results from the graphs show an inverse relationship between the relative pressure and the volume. At low relative pressure (P/P_0), there is an increase in adsorption volume. Isotherms reach a plateau in the middle and have high relative pressure. This behavior suggests the presence of micropores. The isotherms are further analyzed for pore size

distribution [44].

The SEM images (Figure 9) of all the samples display mesopores with non-uniform intercellular spaces. This shows that the addition of the HBU additives does not affect the morphological structure of the activated carbon [51]. Furthermore, the homogenously mixed AC and HBU allows for integration between EDLC and faradaic processes on the electrode surface thereby enhancing electrochemical performance [44].

Sample	Surface area (m^2 g^{-1})	Pore volume (cm^2 g^{-1})	Pore size (nm)
AC	212	0.09	2.11
HBU889	255	0.13	1.45
HBU888	425	0.16	1.69
HBU680	373	0.14	1.59

Table 1. BET results for surface area, pore volume, and pore size of the samples.

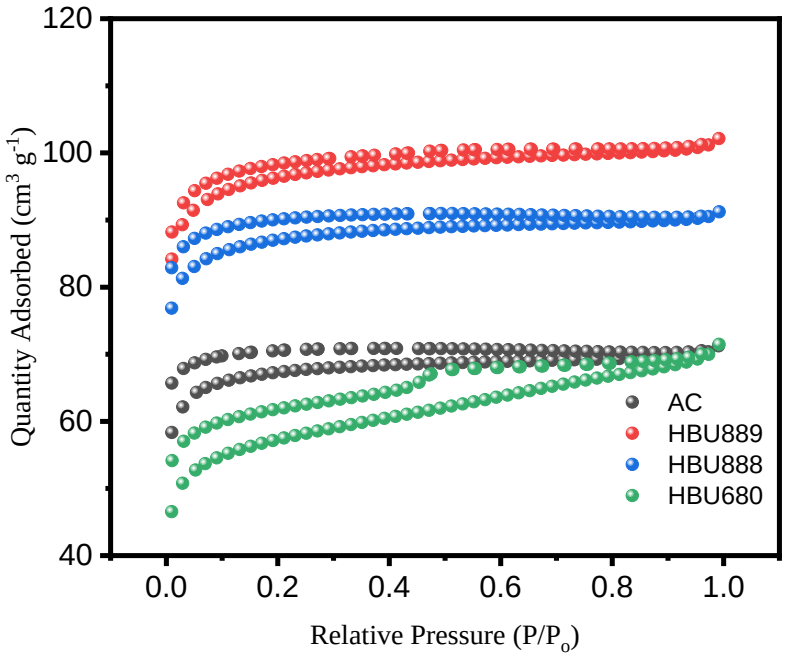

Figure 8. BET N_2 adsorption/desorption for the different samples.

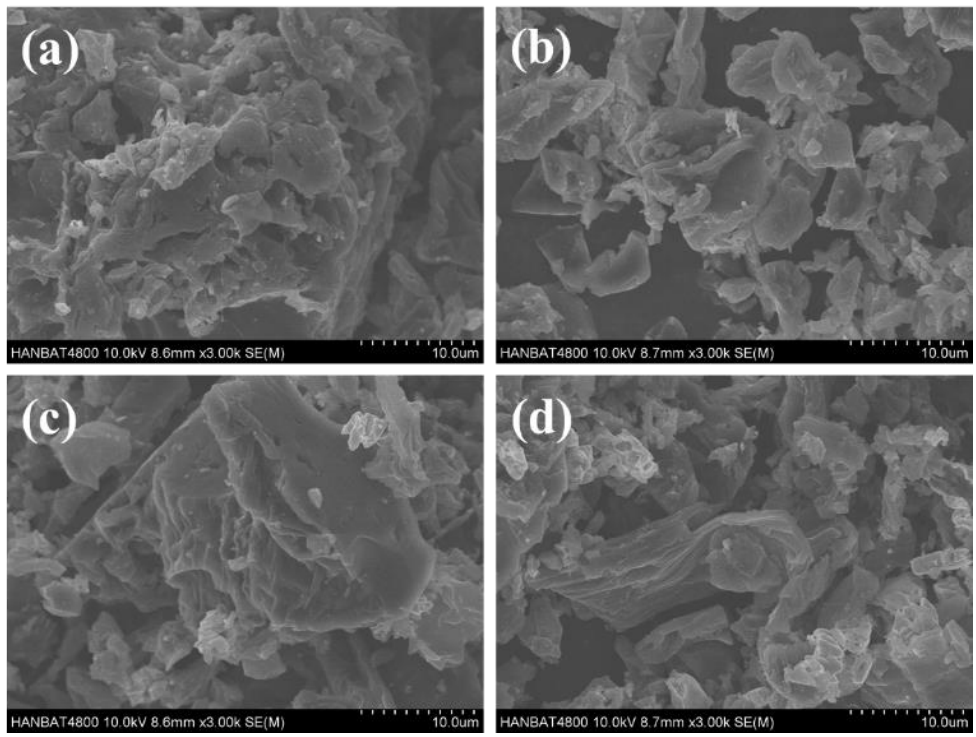

Figure 9. SEM images for (a) AC, (b) HBU 889, (c) HBU 888 and (d) HBU 680.

3.2. Cyclic Voltammetry analysis

The cyclic voltammetry analysis was conducted in a three-electrode cell, which was equipped with a reference electrode made up of Ag/AgCl saturated with KCl, platinum as a counter electrode, and samples (quinone based additives, the activated carbon, and their composites) as a working electrode in an aqueous electrolyte solution of 1 M H_2SO_4 , using an Autolab instrument (PGstat 100, Eco Chemie) at different scan rates of 100 mV/s to 1,000 mV/s at a potential range of −0.2 V to 0.8 V versus Ag/AgCl [57].

Figure 10 and Figure 11 display CV analysis for AC and the three additives HBU 680, HBU 888, and HBU 889. The CVs for the HBU samples show both EDLC behavior and double redox peaks due to the redox reaction of the quinone based additives [58].

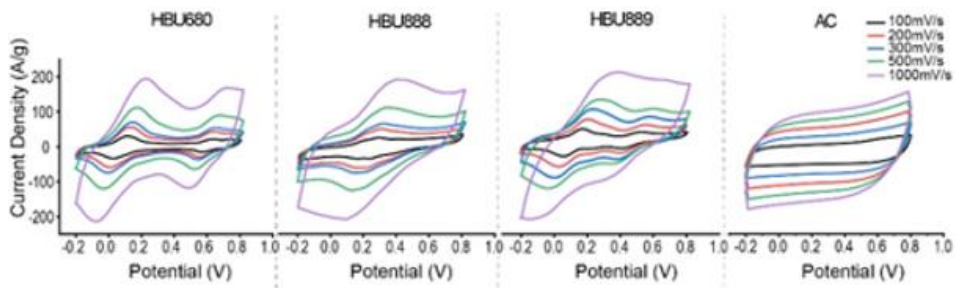

Figure 10. Cyclic voltammograms of AC, HBU 680, HBU 888 and HBU 889 at different scan rate.

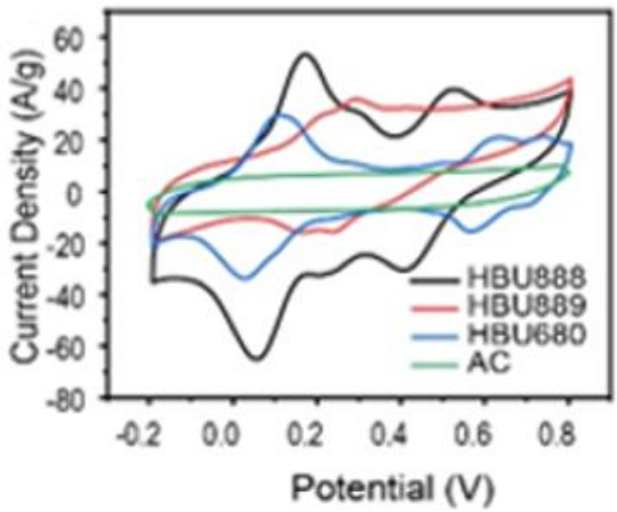

Figure 11. Cyclic voltammograms of all samples at 100 mV/s.

3.3. Galvanostatic charge−discharge

Galvanostatic charge−discharge was carried out at different current densities of 5, 7, and 10 mA/cm^2. All tests were done in the potential range of −0.2 to 1.0 V. Figure 12 and Figure 13 display the Charge−discharge profiles at different current densities and comparison at a current density at a constant current density of 5 mA/cm^2. The HBU 680, HBU 889, HBU 888 and AC had an average charge−discharge time of 141, 129, 391 and 101 s/mg corresponding to specific capacitances 176, 145, 262, and 169 F/g respectively. The HBU 888 had the longest charge/discharge cycle time implying a higher specific capacitance which is in agrees with the CV curves. Furthermore, the HBU888 profile has more defined peak shoulders compared to HBU 680 and HBU 889 implying a more pronounced redox reaction [59].

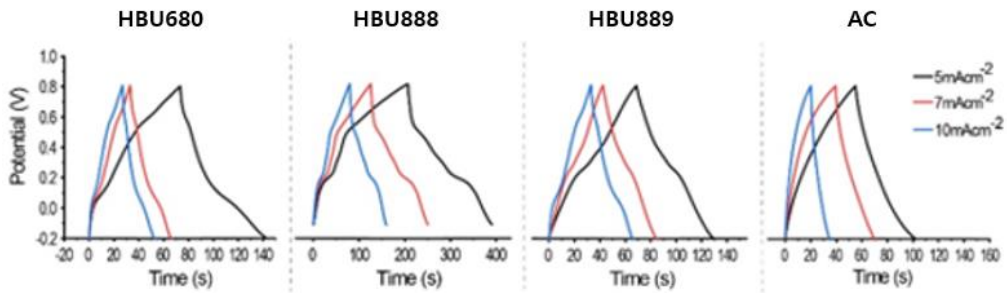

Figure 12. Charge-discharge profiles of supercapacitor electrodes of all samples at a different current density.

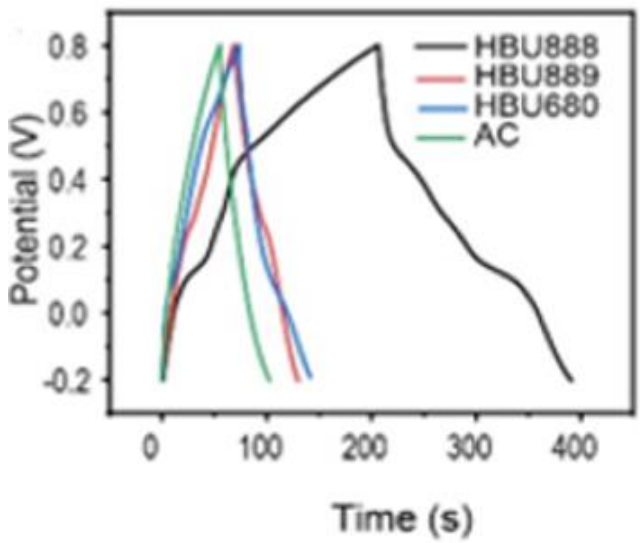

Figure 13. Charge-discharge comparison at current density 5 mA/cm^2.

3.4. Specific capacitance

Table 2. shows the pure AC has the lowest specific capacitance because it only has the EDLC process [60]. However, the combination of AC and the HBU additives produces pseudocapacitive behavior. The HBU additives can homogenize with the AC particles due to formation of intermolecular forces of attraction between the HBU molecules and the surface of the activated carbon, that contains other functional groups such as amine, hydroxyl, carboxylic, carbonyl and aromatic groups. This helps to merge the EDLC and faradaic process within the electrode resulting in improved electron delocalization and charge transfer kinetics [51, 61]. These results suggest that the new HBU additives can enhance the specific capacitance of AC with HBU 888 having the best performance. The ability of the HBU additives to (i) bind to the surface of the AC by forming electrostatic forces of attraction, enhances the cooperation of the EDLC and faradaic process and (ii) undergo fast redox reaction enables then to positively influence the electrochemical properties of the composite electrodes.

Sample	Specific Capacitance @100mVs^{-1}
HBU888	262
HBU889	145
HBU680	176
AC	83

Table 2. Summary of specific capacitance at 100 mV/s.

Chapter 4. Conclusion

The new quinone based electrode additives HBU 680, HBU 889, and HBU 889 were synthesized and used as additives for supercapacitor electrodes. The HBU 680 was characterized by redox reactions of the NH group in the triazole ring and the oxide ion, HBU 889 has $Q-QH_2$ transitions whilst HBU 888 undergoes the $PhQ-PhQH_2$ transition. The galvanostatic results obtained showed that the HBU 888 was the ideal organic additive as it had the longest cycle time which was more than double that of HBU 889 and HBU 680. This study shows that chemically synthesized organic additives have a positive effect on the specific capacitance in supercapacitors. Thus, they are promising candidates for use as electrode additives.

References

1. Berndt, D., & Spahrbier, D. (2000). Batteries, 1. General, in: Ullmann's Encyclopedia of Industrial Chemistry.
2. González, A., Goikolea, E., Barrena, J.A., & Mysyk, R. (2016). Review on supercapacitors : Technologies and materials. *Renewable and Sustainable Energy Reviews*, *58*, 1189–1206.
3. Winter, M. & Brodd, R. J. (2004). What Are Batteries, Fuel Cells, and Supercapacitors?. *Chemical Reviews*, *104*, 4245–4270.
4. Noori, A., El–Kady, M. F., Rahmanifar, M. S., Kaner, R. B., & Mousavi, M. F. (2019). Towards establishing standard performance metrics for batteries, supercapacitors and beyond. *Chem. Soc. Rev., 48(5)*, 1272–1341.
5. Yan, J., Wang, Q., Wei, T., & Fan, Z. (2014). Recent advances in design and fabrication of electrochemical supercapacitors with high energy densities. *Adv. Energy Mater., 4(4)*, 1300816.
6. Yu, A., Chen, Z., Maric, R., Zhang, L., Zhang, J., & Yan, J. (2015). Electrochemical supercapacitors for energy storage and delivery: advanced materials, technologies and applications. *Appl. Energy, 153*, 1–2.

7. Shao, Y., El-Kady, M. F., Sun, J., Li, Y., Zhang, Q., Zhu, M., Wang, H., Dunn, B., & Kaner, R. B. (2018). Design and mechanisms of asymmetric supercapacitors. *Chem. Rev., 118(18)*, 9233-9280.
8. Attia, S. Y., Barakat, Y. F., Hassan, H. H., & Mohamed, S. G. (2020). A single-step synthesis and direct growth of microspheres containing the nanoflakes-like structure of $Zn_{0.76}Co_{0.24}S$ as a high performance electrode for supercapacitors. *J. Energy Storage., 29*, 101349.
9. Conway, B. E. (1991). Transition from "supercapacitor" to "battery" behavior in electrochemical energy storage. *J. Electrochem. Soc., 138(6)*, 1539.
10. Sharma, K., Arora, A., & Tripathi, S. K. (2019). Review of supercapacitors: materials and devices. *J. Energy Storage., 21,* 801-825.
11. Simon, P., & Gogotsi, Y. (2008). Materials for electrochemical capacitors. *Nature Mater., 7*, 845-854.
12. Wang, Y., Song, Y., & Xia, Y. (2016). Electrochemical capacitors: mechanism, materials, systems, characterization and applications. *Chem. Soc. Rev., 45(21)*, 5925-5950.
13. Thierry, B., Daniel, B., & Jeffrey, W. L. (2015). To Be or Not To Be Pseudocapacitive?. *Journal of The Electrochemical*

Society, 162 (5), A5185-A5189.

14. Zhao, X., Sánchez, B. M., Dobson, P. J., & Grant, P. S. (2011). The role of nanomaterials in redox-based supercapacitors for next generation energy storage devices. *Nanoscale, 3(3)*, 839-855.

15. Seker, E., Reed, M. L., & Begley, M. R. (2009). Nanoporous gold: fabrication, characterization, and applications. *Materials, 2(4)*, 2188- 2215.

16. Tianyu, L., Lauren, F., Minghao, Y., Hanyu, W., Teng, Z., Xihong, L., Yexiang, T., & Yat, L. (2014). Polyaniline and Polypyrrole Pseudocapacitor Electrodes with Excellent Cycling Stability. *Nano Lett. 14(5)*, 2522–2527.

17. Chen, G. Z. (2017). Supercapacitor and supercapattery as emerging electrochemical energy stores. *Int. Mater. Rev., 62(4),* 173-202.

18. Long, J. W., Brousse, T., & Bélanger, D. (2015). Electrochemical capacitors: fundamentals to applications. *J. Electrochem. Soc., 162(5)*, Y3.

19. Nomotoa, S., Nakata, H., Yoshioka, K., Yoshida, A., & Yoneda, H. (2001). Advanced capacitors and their application. *Journal of Power Sources, 97-98,* 807-811.

20. Zhang, L. L., & Zhao, S. S. (2009). Carbon-based materials as supercapacitor electrodes. *Chem. Soc. Rev., 38*, 2520-2531.

21. An, K. H., Kim, W. S., Park, Y. S., Choi, Y. C., Lee, M. S., Chung, D. C., Bae, D. J., Lim, S. C., & Lee, Y. H. (2001). Supercapacitors Using Single-Walled Carbon Nanotube Electrodes. *Advanced Materials, 13(7)*, 497-500.

22. Hu, C. C., Chang, K. H., Lin, M. C., & Wu, Y. T. (2006). Design and Tailoring of the Nanotubular Arrayed Architecture of Hydrous RuO_2 for Next Generation Supercapacitors. *Nano Lett., 6*, 2690.

23. Zhang, H., Cao, G., Wang, Z., Yang, Y., Shi, Z., & Gu, Z. (2008). Growth of Manganese Oxide Nanoflowers on Vertically-Aligned Carbon Nanotube Arrays for High-Rate Electrochemical Capacitive Energy Storage. *Nano Lett., 8*, 2664.

24. Choi, D., Blomgren, G. E., & Kumta, P. N. (2006). Fast and Reversible Surface Redox Reaction in Nanocrystalline Vanadium Nitride Supercapacitors. *Adv. Mater., 18*, 1178.

25. Fan, L. Z., Hu, Y. S., Maier, J., Adelhelm, P., Smarsly, B., & Antonietti, M. (2007). High Electroactivity of Polyaniline in Supercapacitors by Using a Hierarchically Porous Carbon Monolith as a Support. *Adv. Funct. Mater., 17*, 3083.

26. Seredych, M., Hulicova-Jurcakova, D., Lu, G. Q., & Bandosz, T. J. (2008). Surface functional groups of carbons and the effects of their chemical character, density and accessibility to ions on electrochemical performance. *Carbon, 46*, 1475.

27. Waseem, R., Faizan, A., Nadeem R., Yiwei, L., & Ki-Hyun, K. (2018). Recent advancements in supercapacitor technology. *Nano Energy, 52,* 441-473.

28. Nathalie, D., Samir, J., Marie-Cecile, P., & Daniel, B. (2014). Review of characterization methods for supercapacitor modelling. *Journal of Power Sources, 246*, 596-608.

29. Qu, D., & Shi, H. (1998). Studies of activated carbons used in double-layer capacitors. *J. Power Sources, 74,* 99.

30. Endo, M., Maeda, T., Takeda, T., Kim, Y. J., Koshiba, K., Hara, H., & Dresselhaus, M. S. (2001). Capacitance and Pore-Size Distribution in Aqueous and Nonaqueous Electrolytes Using Various Activated Carbon Electrodes. *J. Electrochem. Soc., 148,* A910.

31. Raymundo, E., Kierzek, K., Machnikowski, J., & Beguin, F. (2006). Relationship between the nanoporous texture of activated carbons and their capacitance properties in different electrolytes. *Carbon, 44,* 2498.

32. Barbieri, O., Hahn, M., Herzog, A., & Kotz, R. (2005). Capacitance limits of high surface area activated carbons for double layer capacitors. *Carbon, 43*, 1303.

33. Kierzek, K., Frackowiak, E., Lota, G., Gryglewicz, G., & Machnikowski, J. (2004). Electrochemical capacitors based on highly porous carbons prepared by KOH activation. *Electrochim. Acta, 49,* 515.

34. Salitra, G., Soffer, A., Eliad, L., Cohen, Y., & Aurbach, D. (2000). Carbon Electrodes for Double-Layer Capacitors I. Relations Between Ion and Pore Dimensions. *J. Electrochem. Soc., 147,* 2486.

35. Raymundo, E., Leroux, F., & Beguin, F. (2006). A High-Performance Carbon for Supercapacitors Obtained by Carbonization of a Seaweed Biopolymer. *Adv. Mater., 18,* 1877.

36. Pandolfo, A. G., & Hollenkamp, A. F. (2006). Carbon properties and their role in supercapacitors. *J. Power Sources, 157,* 11.

37. Rike, Y., Holia O., Yukie, S., Tadahisa, I., & Jun-ichi, A. (2011). Analysis of Functional Group Sited on Multi-Wall Carbon Nanotube Surface. *The Open Materials Science Journal, 5,* 242-247.

38. Futaba, D. N., Hata, K., Yamada, T., Hiraoka, T., Hayamizu, Y., Tanaike, O., & Hatori, H. (2006). Shape-engineerable and

highly densely packed single-walled carbon nanotubes and their application as super-capacitor electrodes. *Nat. Mater., 5,* 987.

39. Frackowiak, E., Jurewicz, K., Delpeux, S., & Beguin, F. (2001). Supercapacitors from nanotubes/polypyrrole composites. *J. Power Sources, 97-98*, 822.

40. Yoo, J. J., Balakrishnan, K., Huang, J., Meunier, V., Sumpter, B. G., Srivastava, A., Conway, M., Reddy, A. L. M., Yu, J., Vajtai, R., & Ajayan, P. M. (2011). Ultrathin Planar Graphene Supercapacitors. *Nano Lett., 11,* 1423-1427.

41. Zhang, Y., Feng, H., Wu, X., Wang, A., Zhang, T., & Dong, H. (2009). Progress of electrochemical capacitor electrode materials: A review. *int. J of hydrogen energy, 34,* 4889-4899.

42. Ko, J. M., Nam, J. H., Won, J. H., & Kim, K. M. (2014). Supercapacitive properties of electrodeposited polyaniline electrode in acrylic gel polymer electrolytes. *Synth. Met., 189,* 152-156.

43. Hepowit, L. R., Kim, K. M., Kim, H. S., Ryu, K. S., Lee, Y. M., & Ko, J. M. (2012). Supercapacitive properties of electro-deposited polypyrrole on acrylonitrile-butadiene rubber as a flexible current collector. *Polym. Bull., 69,* 873-880.

44. Hu, C. C., & Lin, J. Y. (2002). Effects of the loading and polymerization temperature on the capacitive performance of polyaniline in $NaNO_3$. *Electrochim. Acta, 47,* 4055-4067.

45. Suematsu, S., & Katsuhiko, N. (2001). Quinone-introduced oligomeric supramolecule for supercapacitor, *J. Power Sources, 97-98,* 816-818.

46. Song, Z., & Haoshen, Z. (2013). Towards sustainable and versatile energy storage devices: an overview of organic electrode materials. *Energy Environ. Sci., 6*, 2280-2301.

47. Pognon, G., Thierry, B., Laurent D., & Daniel B. (2011). Performance and stability of electrochemical capacitor based on anthraquinone modified activated carbon. *J. Power Sources, 196*, 4117-4122.

48. Rodney, D. L. S., & Peter, G. P. (2009). Voltammetric quantification of the spontaneous chemical modification of carbon black by diazonium coupling. *Electrochimica Acta, 54*, 2305-2311.

49. Lee, W., Suzuki, S., & Miyayama, M. (2014). Electrochemical Properties of Poly(Anthraquinonyl Sulfide)/Graphene Sheets Composites as Electrode Materials for Electrochemical Capacitors, *Nanomaterials, 4*, 599-611.

50. Alejandro, M., Suheda, I., & Raul, D. (2013). Influence of Impregnation of Activated Carbon Electrodes with p-Benzoquinone on Supercapacitor Performance. *Electrochemistry, 81,* 853-856.

51. Lee, H. S., Latifatu, M., Park, J. H., Lee, Y. G., & Ko, J. M. (2016). Supercapacitive properties of composite electrodes consisting of activated carbon and 1,4-dihydroxynaphthalene derivatives. *Synth. Met., 217*, 29-36.

52. Akai, N., Kawai, A., & Shibuya, K. (2011). Water assisted photo-oxidation from hydroquinone to p-benzoquinone in a solid Ne matrix. *Journal of Photochemistry and Photobiology A: Chemistry, 223*, 182-188.

53. Quan, M., Sanchez, D., Mark, F., & Diane, K. (2007). Voltammetry of quinones in unbuffered aqueous solution: Reassessing the roles of proton transfer and hydrogen bonding in the aqueous electrochemistry of quinones. *J. Am. Chem. Soc., 129,* 12847-12856.

54. Jiang, Y., & Liu, J. (2019). Definitions of Pseudocapacitive Materials: A Brief Review. *Energy Environ. Mater., 2*, 30-37.

55. Won, J. H., Lee, H. S., Hamenu, L., Latifatu, M., & Ko, J. M. (2016). Improvement of low-temperature performance by adopting polydimethylsiloxane-g-polyacrylate and lithium

modified silica nanosalt as electrolyte additives in lithium-ion batteries. *J. Ind. Eng. Chem., 37*, 325-329.

56. Ko, J. S., Sassin, M. B., Rolison, D. R., & Long, J. W. (2018). Deconvolving double-layer, pseudocapacitance, and battery-like charge-storage mechanisms in nanoscale $LiMn_2O_4$ at 3D carbon architectures. *Electrochim. Acta., 275*, 225-235.
57. Kim, K. M., Lee, Y. G., Park, J. H., & Ko, J. M. (2016). Supercapacitive Properties of Composite Electrode Consisting of Activated Carbon and Di(1-aminopyrene) quinone. *ETRI Journal, 38*, 2.
58. Paul, L. K., Scott, H., & Labes, M. M. (1964). Composition of some conducting complexes of 1,6-diaminopyrene. *J. Chem. Phys., 40*, 890-894.
59. Liu, X., Ding, Z., He, Y., Xue, Z., Zhao, X., & Lu, X. (2010). Electrochemical behavior of hydroquinone at multi-walled carbon nanotubes and ionic liquid composite film modified electrode. *Colloids Surfaces B : Biointerfaces., 79*, 27-32.
60. Souier, T., Santos, S., Ghaferi, A. A., Stefancich, M., & Chiesa, M. (2012). Enhanced electrical properties of vertically aligned carbon nanotube-epoxy nanocomposites with high packing density. *Nanoscale Res. Lett., 7*, 1-8.

61. Gao, Y. (2017). Graphene and polymer composites for supercapacitor applications: a review. *Nanoscale Res. Lett., 12*, 387.

국문 초록

축전용량 향상을 위한 퀴논 기반 새로운 전극 첨가제 개발

이 규 철
나노융합전공
융합과학부
서울대학교 융합과학기술대학원

산화환원 활성 유기 화합물은 스위치, 분자 와이어, 센서 및 중요하게는 전자/광전자 장치의 기능성 재료로 입증되었다. 이러한 유기 분자는 산화 환원 반응을 겪을 수 있는 다양한 산화 환원 활성 물질로 기능 화된다. 이들 화합물 중 퀴논계 물질은 합리적인 비용과 친환경적이며 높은 가역성을 나타내어 에너지 저장 장치용 전극 물질로 상당한 주목을 받고 있다. 퀴논과 그 유도체는 전기화학 분야의 유망한 유기 물질이다.

본 연구에서는 퀴논계 유도체를 합성한 후 활성탄과 물리적으로

혼합하였다. 3개의 퀴논계 유도체(HBU 680, HBU 888 및 HBU 889)가 합성되어 슈퍼커패시터용 전극 첨가제로 사용된다. 활성탄 및 그 착물을 포함한 유기 첨가제는 주로 2개의 전자, 2개 양성자 과정을 포함하는 PhQ−$PhQH_2$ 산화환원 전이를 특징으로 한다. 복합 전극은 전류 밀도 5 mA/cm^2에서 HBU 680, HBU 888 및 HBU 889에 대해 각각 176 F/g, 262 F/g 및 145 F/g의 비정전용량을 나타낸다. 사이클 성능 또한 복합 전극의 패킹 밀도를 증가시키기 위해 기공 충전 형태에 $PhQH_2$ 기반 유기 첨가제를 채택함으로써 향상될 수 있다. 복합 전극은 10000회 주기 동안 100% 용량 유지를 보였고 이러한 결과는 새로운 퀴논 기반 유도체가 의사용량성 거동을 향상시킴으로써 슈퍼커패시터용 전극 첨가제로서의 사용을 보증할 수 있음을 보여준다.

퀴논 유도체는 덜 유해한 유기 용매를 사용하여 간단한 1 또는 2단계 합성 공정으로 얻었다. 활성탄을 활물질로, 퀴논 유도체를 산화환원 첨가제로, polyvinylidene fluoride을 고분자 바인더로, N−methyl−2−pyrrolidinone을 분산 용매로 사용하는 코팅 슬러리를 완벽하게 혼합하여 우수한 복합 전극을 제조하였고 SEM을 통하여 확인하였다. 1M H_2SO_4 용액에 복합전극을 작업전극으로 사용하여 Ag/AgCl 기준 −0.2~0.8V의 넓은 전위창에서 cyclic voltammety를 확인한 결과 우수한 용량 유지율을 나타냈다. 이러한 결과는 복합 전극의 정전 용량 성능이 활성탄과 유기 첨가제 사이의 시너지 효과에 기인한다는 것을

보여주었다. 이 효과적인 방법을 통해 슈퍼커패시터로서 우수한 성능의 복합 전극을 얻을 수 있음을 확인했다.

주요어 : 퀴논 기반, 활성 탄소, 산화/환원 반응, 축전용량

학 번 : 2017-22884